sciendo

PRODUCTION ENGINEERING ARCHIVES 2024, 30(3), 361-376

PRODUCTION ENGINEERING ARCHIVES

ISSN 2353-5156 (print)
ISSN 2353-7779 (online)

Exist since 4th quarter 2013
Available online at https://pea-journal.eu

Surface Layer Performance of Low-Cost 3D-Printed Sliding Components in Metal-Polymer Friction

Daniel Pieniak[1], Remigiusz Michalczewski[1], Marcel Firlej[2], Zbigniew Krzysiak[3,7], Krzysztof Przystupa[4,5*], Marek Kalbarczyk[1], Edyta Osuch-Słomka[1], Andrzej Snarski-Adamski[1,3], Leszek Gil[6], Maria Seykorova[7]

[1] Tribology Center, Łukasiewicz Research Network-Institute for Sustainable Technologies (L-ITEE), ul. Pułaskiego 6/10, 26-600 Radom, Poland; daniel.pieniak@itee.lukasiewicz.gov.pl (DP); remigiusz.michalczewski@itee.lukasiewicz.gov.pl (RM); marek.kalbarczyk@itee.lukasiewicz.gov.pl (MK); edyta.slomka@itee.lukasiewicz.gov.pl (EOS); andrzej.snarski@ itee.lukasiewicz.gov.pl (ASA)
[2] Department of Craniofacial Anomalies, Poznan University of Medical Sciences, Bukowska 70, 60-812 Poznan, Poland; marcel-firlej@wp.pl,
[3] Department of Mechanical Engineering and Automation, Faculty of Production Engineering, University of Life Sciences in Lublin, Głęboka 28, 20-612 Lublin, Poland; zbigniew.krzysiak@up.lublin.pl,
[4] Department of Automation, Lublin University of Technology, Nadbystrzycka 36, 20-618 Lublin, Poland; k.przystupa@pollub.pl,
[5] Vilnius Gediminas Technical University, Saulėtekio al. 11, LT-10223 Vilnius, Lithuania,
[6] Faculty of Transport and Computer Science, WSEI University, Projektowa 4, 20-209 Lublin, Poland; leszek.gil@wsei.lublin.pl,
[7] Department of Transport Means and Diagnostics, Faculty of Transport Engineering, University of Pardubice, Studentská 95, 532 10 Pardubice, Czech Republic, marie.sejkorova@upce.cz
* Correspondence: k.przystupa@pollub.pl and zbigniew.krzysiak@up.lublin.pl

Article history
Received 11.12.2023
Accepted 01.06.2024
Available online 09.09.2024

Keywords
polymer materials,
3D DLP printing,
hardness,
wear.

Abstract
The paper presents the results of contact strength and tribological property tests of spare parts made of a popular resin using a 3D DLP printing technology. Two printer models by the same manufacturer were used in the study. The post-processing technique, which shapes the final functional properties, was diversified. Surface performance properties were compared, i.e. Shore hardness, indentation hardness, Martens hardness, elastic modulus, and parameters related to surface creep and relaxation. Tribological durability in rotary motion and tribological wear in reciprocating linear motion were also evaluated using micro- and nanotribometers. This was followed by surface analyses of the friction track of the analysed materials using microscopic methods: a scanning electron microscope, a WLI interferometric microscope, and an optical microscope. The results were statistically processed and the relationship between the parameters determined in the indentation test was determined.

DOI: 10.30657/pea.2024.30.36

1. Introduction

Contact loads are the main cause of friction and wear in components of engineering equipment. They occur, among others, in kinematic machine nodes (Kałdoński, 2020; Lawrowski, 2008; Gil, et al., 2021) and in situations where it is necessary to maintain continuous operational readiness or where damaged core components must be replaced, for example, for regeneration-related reasons. In most cases, such technologies as surfacing (Romek, et al., 2020) or regenerative adhesive composites are used (Smal, 2006); additionally, reverse engineering can and 3D printing directly from a computer-aided design (CAD) model (Dangnan, et al., 2020; Snyder, 2015). Three-dimensional (3D) printing has many potential applications in engineering, such as precision component manufacturing (Figure 1), medical devices (Kim, et al., 2021; Rezaie, et al., 2023), aerospace components (Wang, et al., 2021), marine (Mohammed, et al., 2016) and in particular for the manufacture of components, i.e. lip seals, rollers, ball bearings and artificial joint (Zhang, et al., 2013). Additive manufacturing (AM) of polymeric materials is often used (Ramadan, 2022). AM is a technology that can be used in manufacturing processes with low energy intensity, complex product shapes, low cost, and minimal post-processing (Aziz, et al., 2020). Due to

its speed and low manufacturing costs, a digital ligt processing (DLP) incremental technology, in which polymer resins are cured with light, is often used, particularly to make models and functional products. Given the good structural cohesion, low porosity, relatively high hardness and stiffness, as well as surface quality, small parts operating in precision mechanisms (Figure 1) are produced, and due to the texture, surface type and color, so-called technical plating is produced (Lim, et al., 2022). Along with the development of the 3D polymer printing technology as an industrial manufacturing method, the variety of polymer materials continues to grow and their use in various fields increases. Further development of applications is related to the recognition of the behaviour of a given material in an operational environment (Jandyal, et al., 2022; Mitchell, et al., 2018; Qu, et al., 2023; Topolinski, 1997).

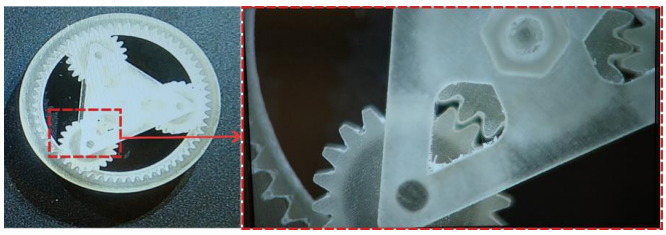

Fig. 1. AM gear elements made of light-cured resin

Tribology of polymers is different from tribology of metals for many reasons. In contrast to metals, polymers are viscoelastic and their properties are dependent on time (Abdelbary, 2014). There are two main non-interacting components of friction, namely, adhesion and deformation. Such approach is correct for any materials including polymers (Myshkin, et al., 2005). This process is similarly described by Kragielski's molecular-mechanical theory, i.e. on the actual contact surfaces of rubbing bodies there are resistances caused by molecular and mechanical interactions caused by the engagement of micro-irregularities on the surfaces of these bodies and their mutual sinking (Lawrowski, 2008). Some research has established that the wear of polymers can be subdivided into three main groups: adhesion, abrasion and surface fatigue (Abdelbary, 2015). According to experimental works, the wear regimes of polymers are strongly affected by both the formation of transfer films and fatigue loading. The transfer film of a polymer has a pronounced effect in determining the mechanisms of sliding, abrasive or adhesive wear (Abdelbary, 2014). In the metal-polymer tribological pairs that are in the scope of this article, the adhesive bonds between the rubbing surfaces determine the physical properties of the formed transfer film and the size of the wear particles. Three factors that determine the transfer of the polymer: deformation of surface asperities under load, fracture of material in the substrate, and the adherence of this material to another surface (Abdelbary, 2015). In the process of friction, transfer film are continuously formed and destroyed (Capanidis, 2013). In the first stage of sliding, called "Running-in", is related to the removal of the "manufacturing" surface of the polymer specimen, which is characterised by highly residual stresses. The second stage has a lower and linear wear rate and is characterised by formation of a stable transfer film layer of polymer, which is worn in a steady and uniform way. The third stage is accelerated wear. (Abdelbary, 2014). At this stage, the effects of fatigue processes, e.g. cracks, are most noticeable. The number of cycles for subsequent stages depends on the technological properties of the surface layer, which is transformed into the operational surface layer in the tribological system (Ozimina, et al., 2013). Sliding fatigue occurs in polymer sliding elements. Fatigue life depends on the strength of the polymer material and the level of fatigue stress. Replacing the original part with a polymer element made using 3D DLP technology while maintaining the same load level may affect the expected operating time. The expected life of a replacement part may be within the low cycle life range.

Core parts operating in kinematic nodes, which are intended for long-term use, are most often made from non-polymeric materials using a removal processing technology. Increasingly, 3D printed polymer parts are used to replace temporarily core parts, for example, in technological machines whose operation is necessary to maintain continuity of production. In such applications, friction and wear are equally important problems. One of the determinants of research is the growing environmental awareness (Aziz, et al., 2020) and the increasing cost of technological materials. Failure to consider tribological properties of materials can lead to increased energy consumption in the friction process and to economic losses (Shafi, et al., 2018). In a paper (Ramadan, 2022), it was found that only 3% of research into printed polymers focused on their tribological properties and 12% — on their mechanical properties (Rouf, et al., 2022). Currently, tribological research on AM polymers focuses on a fused deposition modelling (FDM) technology (Carneiro, et al., 2015; Dawoud, et al., 2015; Mohamed, et al., 2016); there are also papers on materials used in a PolyJet technology (Dangnan, et al., 2020). Only a few papers containing the results of studies on the surface layer properties of parts manufactured using the 3D DLP technology were published (Mohamed, et al., 2017). Therefore, the cognitive objective is one of the main determinants of this paper.

A manufactured spare part, even intended for short term use, must meet specific requirements for which material properties are a critical feature (Ashby, 2011a; LeBlanc, et al., 2023; Rouf, et al., 2022). Material selection must be made early at the conceptual stage of the design process (Ashby, 2011b). The use of 3D printing materials and technology is an alternative approach and can be successfully used to reproduce components damaged (e.g. worn out) in the operational process. However, as in the case of other technologies, the basic selection criteria for the 3D printing technology are the same. The material must carry mechanical loads for a certain period of time and be resistant to external factors like temperature or moisture. In many technical applications, the resistance of component’s surface is crucial. Particularly susceptible to damage are kinematic nodes of machines and micro-machines where sliding friction occurs. These may include joints, guides, plain bearings or transmission elements (Skoć, et al., 2008). In such nodes, not only wear resistance is important, but also the friction coefficient, especially under dry friction conditions (Krzyzak, et al., 2023). This issue is particularly

important in mechanical systems where no external grease or lubricating oil is used (Carneiro, et al., 2015). It is also known that the components of a friction node should be selected so that they have low adhesive affinity (they should be made of different chemically and/or structurally diverse materials) (Skoć, et al., 2008). This provides a basis for the use of the 3D DLP technology to produce polymeric parts that cooperate with metal components. Unfortunately, in most cases, resin and 3D printer manufacturers do not specify the surface properties of materials used. In-service experience shows that there are large differences in the damage resistance and durability of spare parts. Also, researchers found that no single polymer behaves optimally under certain tribological conditions (Wang, et al., 2016). Therefore, the utilitarian goal of the work is to recognize the tribological behavior of parts manufactured using the DLP method from a low-cost popular material under various friction and wear modes.

The hypothesis is that performance properties of manufactured parts do not significantly vary depending on the type of a printing device and exposure time in post-processing.

2. Materials and methods

2.1. Materials

Phrozen Beige Standard (PBS) material was used in the study. It is a light-curing material with a density of 1.14 g/cm^3, tensile strength of 51 MPa, elastic modulus of 980 MPa and Shore hardness of 72 ShD (www.3dpartnershop, november 2023). Two 3D printers using an SLA/DLP (Stereolithography/Digital Light Processing) technology were used in the study. This technology employs successive layers of an additively applied material exposed to UV light for curing. The parameters of this process are provided in Table 1. The first device was the Phrozen Shuffle Lite (PSL) (www.fepshop, november 2023a) equipped with a 5.5-inch LCD screen with an XY range of 2560 dpi x 1440 dpi and a resolution of 47µ m (Figure 2a). The Phrozen Sonic Mini (PSM) is a printer characterised by high printing speed (www.3djake, november 2023) and a resolution of 62.5 µm (Figure 2b).

Table 1. 3D printing and processing parameters for test samples

Parameter	Sample group 1	Sample group 2	Sample group 3
Material (light-curable resin)	PBS	PBS	PBS
3D printer	PSL	PSM	PSM
Thickness of the normal print layer	50 mµ	50 mµ	50 mµ
Number of bottom layers	6	6	6
Exposure time of the bottom layer	60 sec	25 sec	25 sec
Exposure time of normal layers	10 sec	2.5 sec	2.5 sec
Rinse time in isopropyl alcohol 99%	6 sec	6 sec	6 sec
Exposure time in AWC device	12 min	4 min	12 min

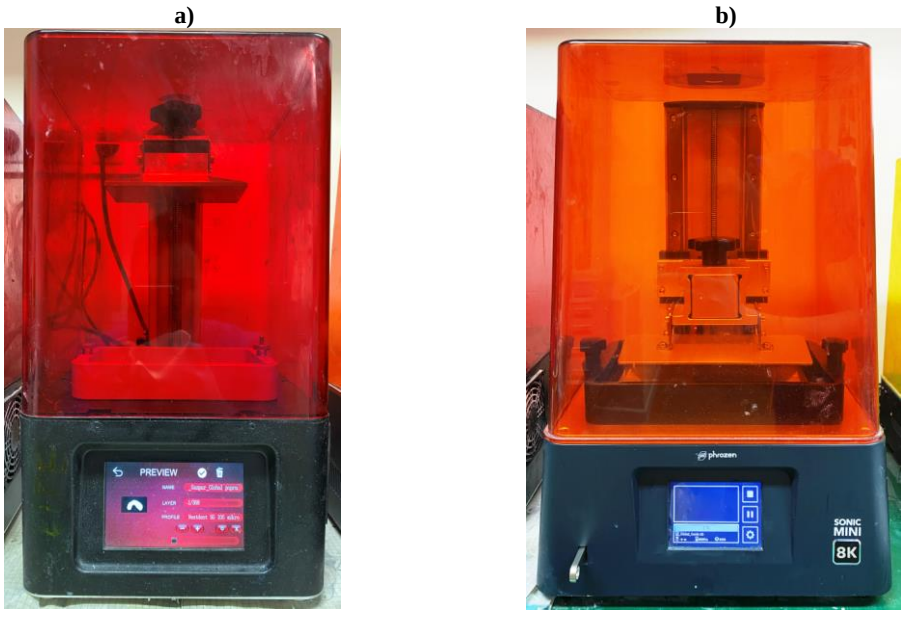

Fig. 2. Photos of 3D printers using SLA/DLP technology: **(a)** Phrozen Shuffle Lite, **(b)** Phrozen Sonic Mini

Post-processing of material samples was carried out in the Anycubic wash and cure (AWC) device (Figure 3) (www.phrozen3d, november 2023), which supports 3D printers with SLA, LCD and DLP technologies. The device uses 99% isopropanol alcohol as a cleaning agent. The samples are washed by rotation. In addition, the procedure of

drying with a stream of hot air and curing the product cleaned in the cleaning process with UV light lamps equipped with lenses that disperse light uniformly (wavelength of 405 nm) is carried out. In the study, the numerical designation of samples was used, e.g. 6/4. The first number is the rinse (wash) time in isopropyl alcohol, which was 6 min; number 4 (or 12) indicates the exposure (cure) time in minutes. Detailed parameters of sample processing are given in Table 1.

Fig. 3. Image of the wash and cure machine

The samples, as delivered to the laboratory, are presented in Figure 4. Samples were made in the shape of discs and cuboids (plates). A minimum of four samples (n = 4) of each shape and type of the material tested were made. Discs with a diameter of 30 mm and thickness of 6 mm were used for Shore hardness and tribological wear resistance tests. Cuboids with dimensions of 25 mm x 25 mm x 5 mm were used in indentation hardness tests.

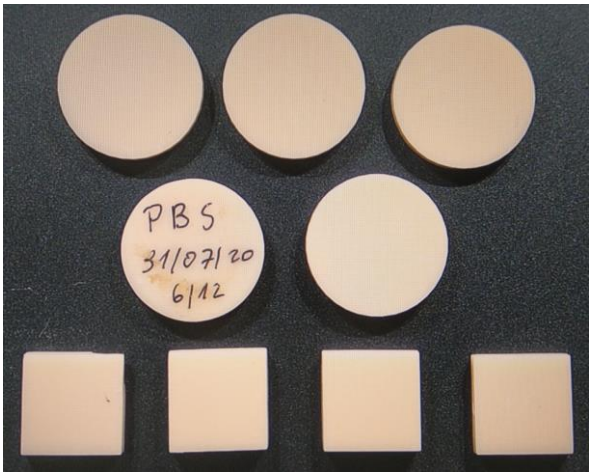

Fig. 4. Image of samples made of the PBS material with the Phrozen Shuffle Lite printer

The surface of samples for indentation hardness and tribological wear tests was machined on laboratory grinder equipped with a Rubin head. The samples were ground with abrasive discs of P600, P1200, P2400 grit and polished with a cloth with a suspension of ceramic particles. Water cooling was used during grinding and polishing.

2.2. Roughness test

The surface roughness of samples was determined using a optical profilometer. The vertical resolution is < 0.01 nm and the horizontal resolution is up to 0.01 m. Based on the geometric surface measurements, the following parameters were calculated described in (ISO 14577; 2015): Sa, , Sku, Sp, Sq, Ssk, Sv. and Sz.

2.3. Shore hardness measurement method

Hardness testing was carried out using a Shore D scale apparatus in accordance with ISO 868:2005 (ISO 868; 2005). This was an durometer mounted on a tripod

2.4. Indentation measurement method

Test was carried out on a Micro Combi Tester (MCT, Anton Paar GmbH, Ostfildern, Germany) (Figure 5). Indentation hardness HV_{IT} and indetation modulus E_{IT} was determined were determined according to the principles described in (Hardiman, et al., 2016; Oliver, et al., 2004; Sneddon; 1965).

Martens hardness is determined by the applied loading force and relates to plastic and elastic deformation. Martens hardness is defined as the quotient of loading force P and indenter area $As(h)$ at depth h (Pokorska, et al., 2014). For the Vickers indenter, Martens hardness is calculated from the equation $HM = P/26.43\ h^{.2}$.

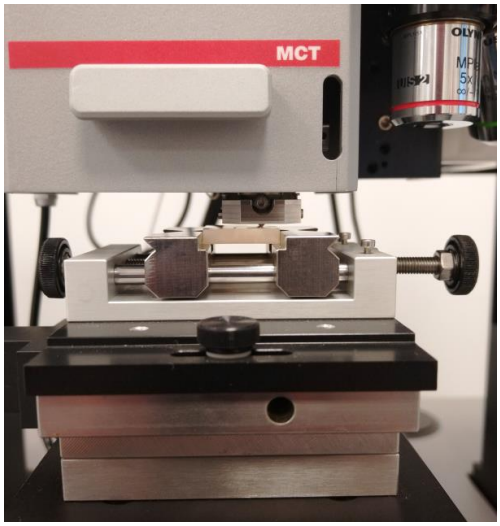

Fig. 5. Indentation hardness measurement

The test additionally determined indentation creep C_{IT}. As defined, the C_{IT} parameter is the change in the indentation depth at constant load in percent and it was calculated using the equation:

$$C_{IT} = \frac{h_2 - h_1}{h_1} \cdot 100 \quad (1)$$

where:
h_1 – the penetration depth at time t_1 after reaching force F (which is maintained constant), and
h_2 – the penetration depth after time t_2 of maintaining force F at a constant level (Figure 6).

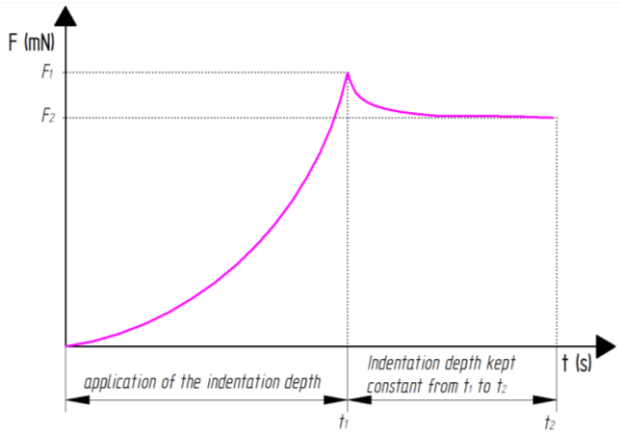

Fig. 6. Diagram of the C_{IT} parameter measurement process

Then, relaxation parameter R_{IT} was determined using the following equation (ISO 14577; 2015):

$$R_{IT} = \frac{F_1 - F_2}{F_1} \cdot 100 \quad (2)$$

In the relaxation parameter equation, F_1 is the force the assumed value of which was reached at the corresponding penetration depth. Then, the indenter was kept at the same depth for the assumed time from t_1 to t_2 (the time is $t_2 - t_1$) until force F_2 was reached (Figure 7).

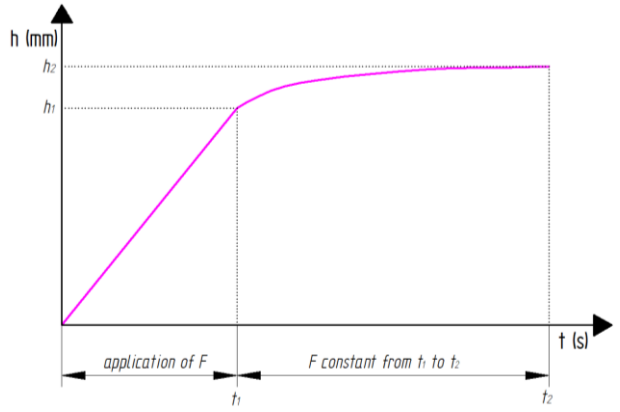

Fig. 7. Diagram of the R_{IT} parameter measurement process

2.5. Durability and linear wear tests in circular sliding friction

Tests under dry sliding friction conditions were conducted on a microtribometer (Figure 8a). A metal ball (ϕ6, 100Cr6 steel)–polymer disc (ϕ30, PBS material) friction pair was used. The loads was 2 N and 20 N. The test was conducted in rotary motion, the radius of friction was 8 mm, and the linear speed was 250 mm/s. The number of friction cycles was set at $20 \cdot 10^3$, which was to correspond to the assumed service life, which according to the literature is classified as Low Cycle Fatigue (LCF) (Müller, et al., 2019). The friction coefficient (μ) and linear wear (Pd) in micrometres were recorded. Durability was defined as the number of friction cycles until the loss of sliding properties (a spike in the friction coefficient) and transition to intensive wear.

2.6. Wear tests in reciprocating linear motion

Tests under dry sliding friction conditions were conducted on a nanotribometer (Figure 8b).

A sinusoidal motion trajectory of the counter sample with a peak-to-peak path value of 6 mm was assumed. A test frequency of 2 Hz and load of 600 mN were assumed. The number of friction cycles was the same as in the circular motion test, i.e. $20 \cdot 10^3$.

a)

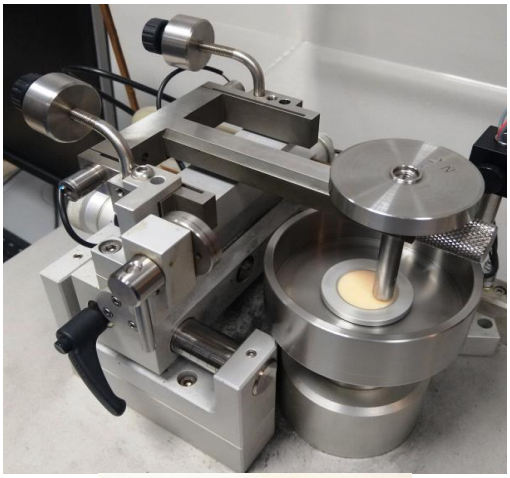

b)

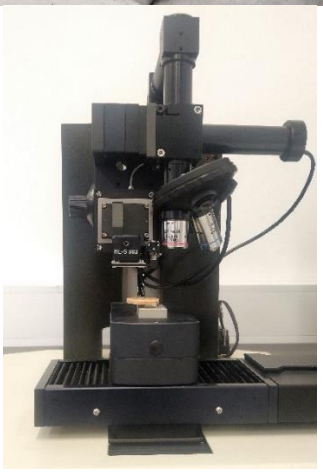

Fig. 8. Tests under dry sliding friction in a metal-polymer system with concentrated contact in rotary **(a)** and reciprocating motion **(b)**

3. Test results

3.1. Shore hardness test results

The Shore hardness test results are shown in a box-plot (Figure 9). This is a graph in which the point represents the median, the box represents the percentiles of 25 and 75, and the whiskers represent the minimum (Min) and maximum (Max) values. The analysis of the graph shows that the highest ShD was found in samples made with the PSL printer. However, the hardness was only slightly higher than that obtained for samples made with the PSM printer.

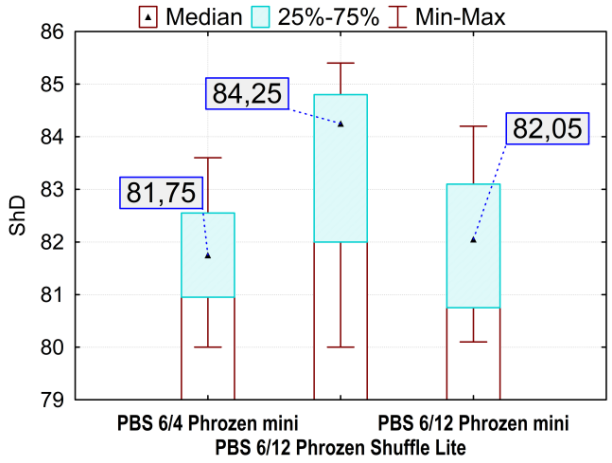

Fig. 9. Box-plot of Shore hardness of the tested materials

3.2. Results of indentation tests

The results of indentation test are presented in Table 2. The statistical distribution values of test results were calculated: mean value (Mean), standard deviation (Std Dev), minimum (Min) and maximum (Max) values.

The analysis of the results in Table 2 shows clear differences in the average HVIT and HM values. For samples made with the PSM printer, not only are they significantly lower, but also different due to the exposure time in the post-processing. However, the differences between the parameter values obtained using the PSM printer are lower. More favourable values of the measured parameters were obtained for samples exposed after cleaning in the AWC device for 4 min, i.e. with a three times shorter additional exposure time.

Table 2. Results of indentation tests with Vickers indenter

Material	PBS 6/4 PSM	PBS 6/12 PSL	PBS 6/12 PSM
		HV_{IT} [HV]	
Mean	4.742	19.422	3.483
Std Dev	0.404	0.338	0.272
Min	4.33	18.722	3.018
Max	5.43	19.881	4.03
N	12	11	13
		E_{IT} [Gpa]	
Mean	2.165	3.717	1.81
Std Dev	0.289	0.115	0.164
Min	1.786	3.584	1.541
Max	2.685	3.88	2.127
N	12	11	13
		HM [Mpa]	
Mean	40.856	141.242	30.479
Std Dev	3.577	1.443	2.343
Min	37.05	138.713	26.801
Max	47.325	143.145	35.327
N	12	11	13
		C_{IT} [%]	
Mean	4.143	2.953	3.46
Std Dev	0.216	0.04	0.079
Min	3.864	2.881	3.344
Max	4.511	3.023	3.616
N	12	11	13
		R_{IT} [%]	
Mean	-0.042	-0.018	-0.042
Std Dev	0.041	0.052	0.066
Min	-0.145	-0.096	-0.16
Max	0.023	0.056	0.032
N	12	11	13

3.3. Surface topography after polishing

Selected surface profiles of tested samples are shown in Figure 10. A selection of topographic charts extracted from a 1 mm x 1 mm plot is presented; the range of the vertical scale (in the direction of the Z axis) was constant between -60 µm and +60 µm, which facilitates comparison of the topographic charts.

a)

b)

c)

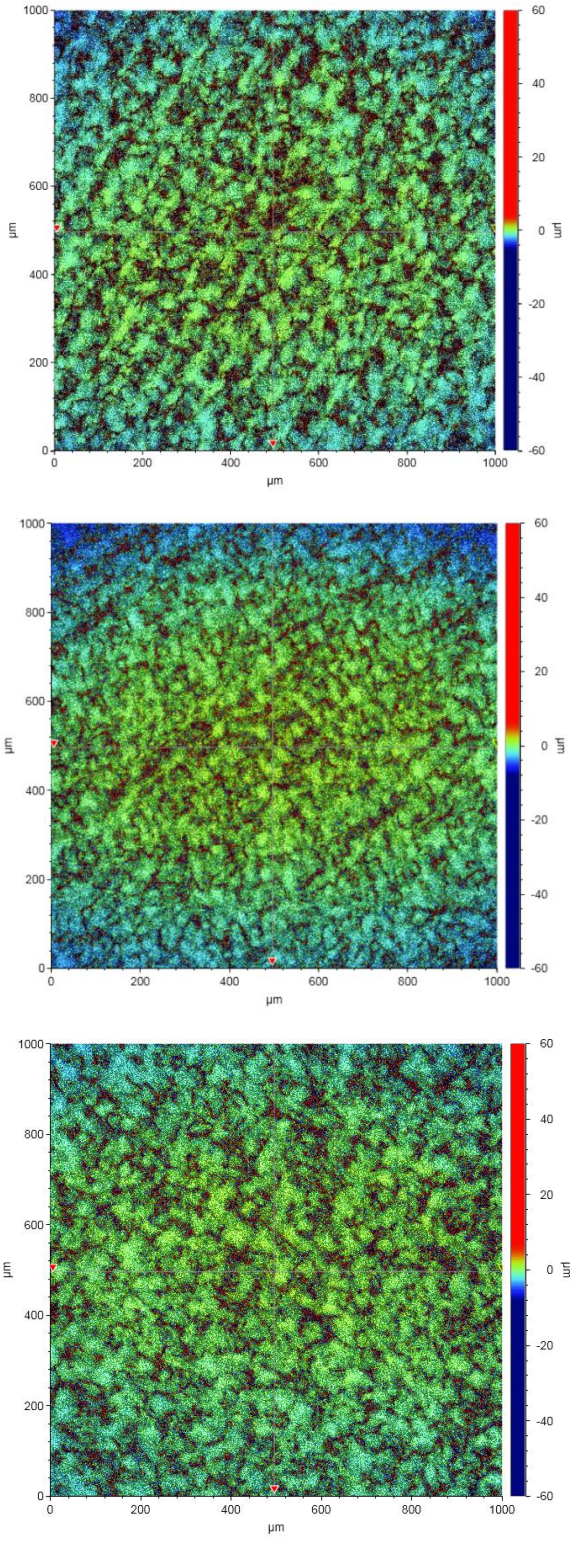

Fig. 10. Surface topography of the tested material samples: **(a)** PBS 6/4 PSM, **(b)** PBS 6/12 PSL, **(c)** PBS 6/12 PSM

Table 3 presents the roughness parameters characterising the friction surface of samples used in tribological durability tests. The highest value of the *Sa* parameter was obtained for the PBS 6/12 PSM sample.

Table 3. Surface roughness parameters of the tested material samples

Materials / Label	PBS 6/4 PSM	PBS 6/12 PSL	PBS 6/12 PSM
Sa	1.82	2.427	2.43
Sku	31.661	24.072	22.338
Sp	52.617	65.054	60.923
Sq	3.609	4.149	4.353
Ssk	1.621	1.268	0.39
Sv	-45.934	-58.824	-58.017
Sz	98.551	122.878	118.94

3.4. Results of linear wear and durability tests

The graph (Figure 11) presents selected results of friction tests in rotary motion. The abscissa shows the number of friction cycles and the ordinate shows the linear wear in micrometres and the friction coefficient (Figure 11). The graph clearly shows the stages of the friction and wear process. There are visible points where a step change in the direction of curves took place. The beginning of the accelerated wear stage and increase in friction coefficient can be identified with the loss of sliding properties by the friction couple.

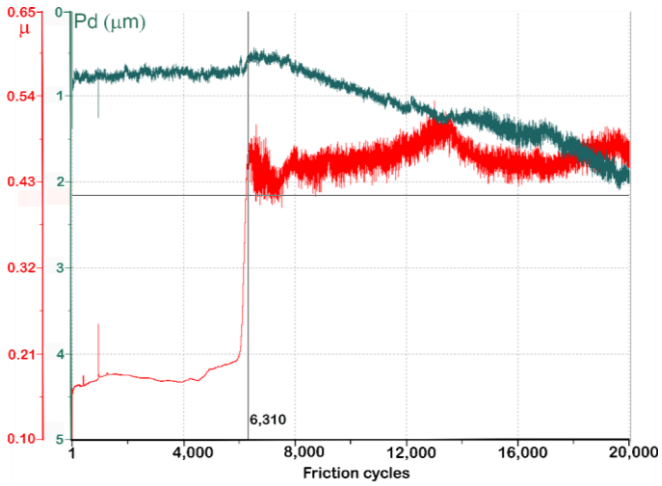

Fig. 11. Friction coefficient (red) and linear wear (green) as a function of friction cycles

Table 4 shows the durability described by the number of friction cycles until the pair loses its sliding properties, depending on the normal force load on the friction node. Two values of the normal force differing by an order of magnitude were assumed.

Table 4. Relationship between friction couple durability and normal load in material groups

Normal force		2 N	20 N
		Durability (Friction cycles)	
Groups	PBS 6/4 PSM	> 20.000	11.800
	PBS 6/12 PSL	6.310	1.200
	PBS 6/12 PSM	1.170	1.100

The results presented in Figure 10 take into account the thermal expansion of the sample and counter sample, and the linear wear is summed for both elements of the friction couple. Considering the above, it was found that under a load of 2 N, the linear wear after $20 \cdot 10^3$ cycles in the steel ball - PBS 6/4 PSM disc friction couple was the lowest. The approximate durability is higher than the assumed number of friction cycles. Under a higher normal load, samples from this material group also showed the highest durability. The most intensive wear was observed in the case of the metal-polymer couple in which the PBS 6/12 PSM group was tested and it was critical. In the test of this group of samples, the target number of test cycles was not achieved. The failure criterion was reached after only about $1 \cdot 10^3$ cycles, and the durability did not vary significantly depending on the load. In addition, the test was not brought to $20 \cdot 10^3$ cycles. It was discontinued after about $3 \cdot 10^3$ cycles, which was justified by the increase in the kinematic coefficient of friction to a value > 1 (Table 5).

Table 5. Descriptive statistics of friction coefficient

Groups	Normal force (N)	COF (μ)				
		Start	Min	Max	Mean	Std Dev
PBS 6/4 PSM	2	0.200	0.144	0.203	0.197	0.006
	20	0.044	0.033	0.829	0.392	0.332
PBS 6/12 PSL	2	0.089	0.089	0.533	0.375	0.129
	20	0.154	0.133	0.649	0.528	0.089
PBS 6/12 PSM	2	0.306	0.306	1.145	0.934	0.274
	20	0.187	0.127	0.812	0.735	0.131

3.5. Results of friction and wear tests in linear reciprocating motion

The graph (Figure 12) presents the results of friction coefficient tests. These are the positive peaks reached in successive friction cycles. The curves of friction coefficient as a function of the number of friction cycles are similar across the test groups, and the most similar in the case of PBS_6/4_mini and PBS_6/12_PSL samples. Table 6 presents the descriptive statistics of friction coefficient test results. The highest mean was observed for the samples made with the Shuffle Lite printer.

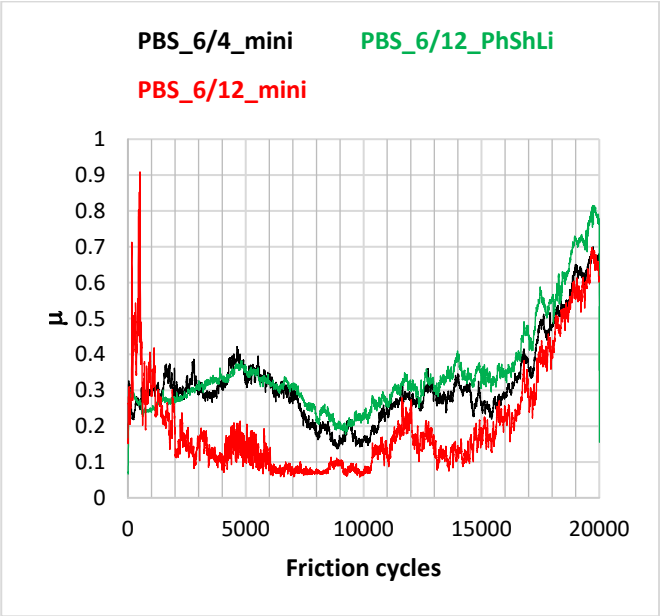

Fig. 12. Peak values of friction coefficient in successive cycles

Table 6. Descriptive statistics of friction coefficient peak values in successive cycles

Groups	COF (μ)			
	Min	Max	Mean	Std Dev
PBS 6/4 PSM	0.056	0.797	0.316	0.133
PBS 6/12 PSL	0.001	0.913	0.351	0.155
PBS 6/12 PSM	0.00001	1.150	0.207	0.172

An isometric view of friction track sections in the middle part is presented in Figure 13. The furrow sections can be seen, which were formed after $20 \cdot 10^3$ cycles for the ball (100Cr6 steel)-disc (PBS polymer material with different configurations of print parameters) friction couple. Figure 14 shows the wear analysis, including measurement plots of the cross-sectional area, width and depth of the friction track made using a White Light Interferometry (WLI) microscope . The analyses identified the material with the highest wear (Table 7). Given the cross-section and depth of friction track, it was the PBS_6/4 mini. However, PBS_6/12 mini had the widest friction track.

In practical evaluation, the synergistic wear of both elements of the kinematic pair is important. Therefore, not only the disc, but also the ball should be assessed. Damage to the metal component should be as low as possible, because in the friction couple under evaluation it is the disc that is made of a material that is intended for spare parts operating within the range of limited durability. This means that the metal part should wear out as little as possible in contact with the polymer component made with the 3D DLP printing technology.

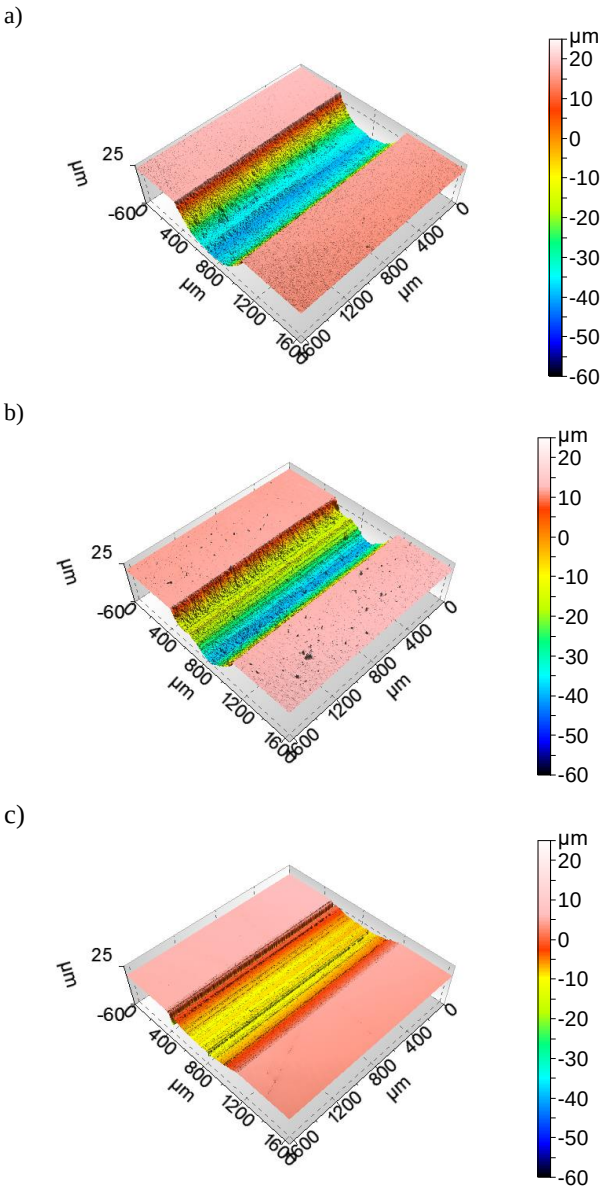

Fig. 13. Comparison of isometric views of friction tracks on the surfaces of the tested material samples:
(a) PBS_6/4_mini, **(b)** PBS_6/12_PSL, **(c)** PBS_6/12_PSM

Tab. 7. Geometrical quantities (mean and standard deviation) characterising wear in the friction track of samples (n = 3)

Groups	Maximum depth	Wear track width	Cross-sectional area of the wear mark
	µm	µm	µm²
PBS 6/4 PSM	57.266 (±0.408)	684.546 (±3.088)	28013.900 (±83.788)
PBS 6/12 PSL	52.035 (±0.304)	641.264 (±1.599)	20044.370 (±289.403)
PBS 6/12 PSM	23.392 (±0.472)	726.798 (±5.612)	8151.310 (±206.543)

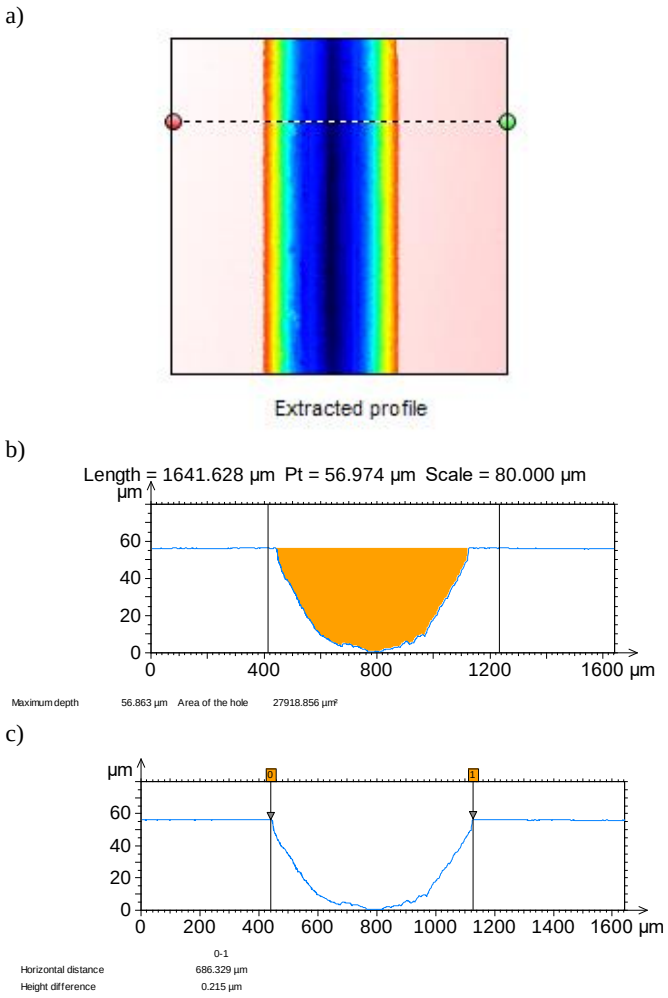

Fig. 14. Wear analysis based on geometric parameters of the friction track **(a)** cross-section, **(b)** the cross-sectional area, **(c)** width of the friction track made using a White Light Inter-ferometry (WLI) microscope

Figure 15 summarises the microphotographs of the friction damage of ball surface depending on the group of PBS material samples. The lowest wear was observed for a ball and PBS 6/4 PSM disc friction couple. This test result in linear oscillatory motion is consistent with the evaluation of linear wear obtained in tests in rotary motion on the microtribometer.

The wear of a ball (counter-sample) in contact with a disc made of PBS 6/12 PSM is the highest. The surface area of the wear mark is so large that it was not possible to capture it in its entirety at the lowest available magnification of an optical microscope. The deep scratches and furrows indicate wear by micro-scraping (Figure 15). This wear is probably caused by a third body, i.e. metal particles removed from the friction surface of the ball, which were present in the friction track between the ball and disc. Such a wear mechanism is also confirmed by SEM/EDS studies conducted using an field emission scanning electron microscope , equipped with an EDS energy dispersive X-ray microanalyzer.

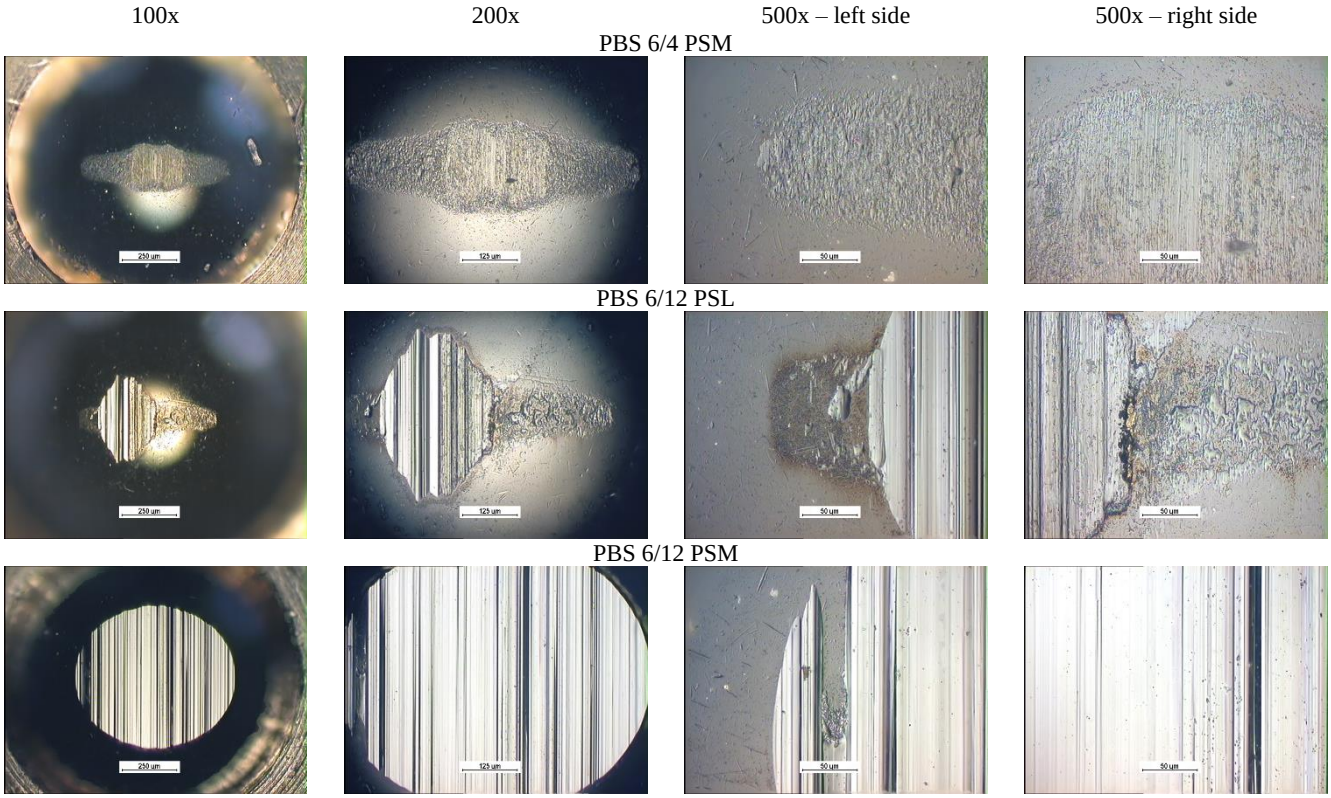

Fig. 15. Wear on the surfaces of counter samples made of 100Cr6 steel

Figure 16 shows the results of quantitative and qualitative EDS analysis of elemental composition from the friction track surface of PBS samples, with the following operating parameters: accelerating voltage 15kV, working distance 30^{O}, and SE detector. Prior to microscopic studies, the surface of samples was sputtered with a 20-nm-thick carbon layer. For this purpose, a sputter coater was used. PBS 6/12 PSM had the highest weight share of iron particles, which could only come from the steel ball. The lowest share was recorded for PBS 6/4 PSM, which corresponded to the friction damage to the balls in each friction couple.

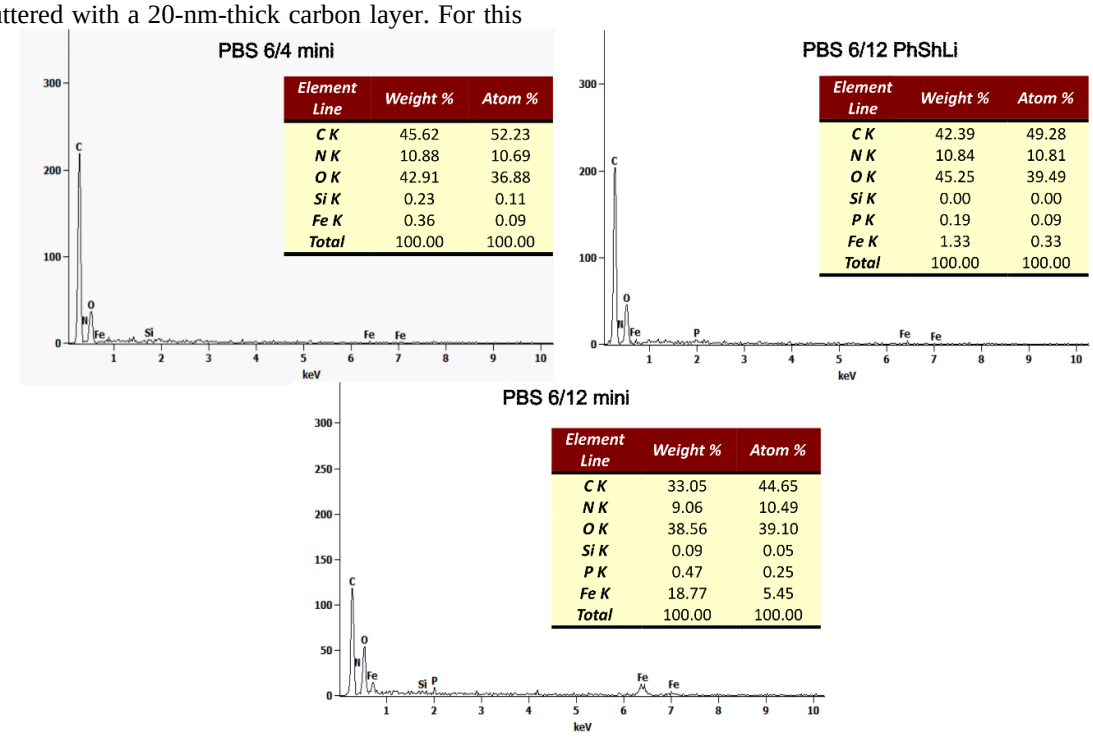

Fig. 16. EDS X-ray spectrum and elemental composition in [at.%] and in [wt.%] from the friction track surface of PBS samples

The authors also analysed whether the measured wear translated into variations in the wear mechanisms of PBS material samples. The results from friction track surface observations are shown in Figure 17 in the form of SEM images taken for the 120 µm x 120 µm area, column one (Figure 17 a,d,g) and 40 µm x 40 µm, columns two and three (Figure 17 b,c,e,f,h,i), using magnifications of 1000x and 3000x, respectively. In the case of 6/4 PSM samples (Figures 17a–17c), a clear separation of particles was observed, and no adhesive or abrasive wear mechanisms were visible. Wear was caused by cyclic load changes. In successive cycles, material particles are separated at the grain boundary and then removed. In addition, agglomerates are visible. It seems that wear products (particles) do not intensify abrasive wear and do not smear. In the case of the 6/12 PSL samples, deformation in the direction of friction and plastic deformation consistent with the direction of friction are visible. Analysis of the friction track of 6/12 PSM samples showed clear fatigue cracks, furrows, probably caused by hard particles, which are products of wear. Smeared material particles were also observed. For these samples, the wear mechanism was clearly different from the other material groups.

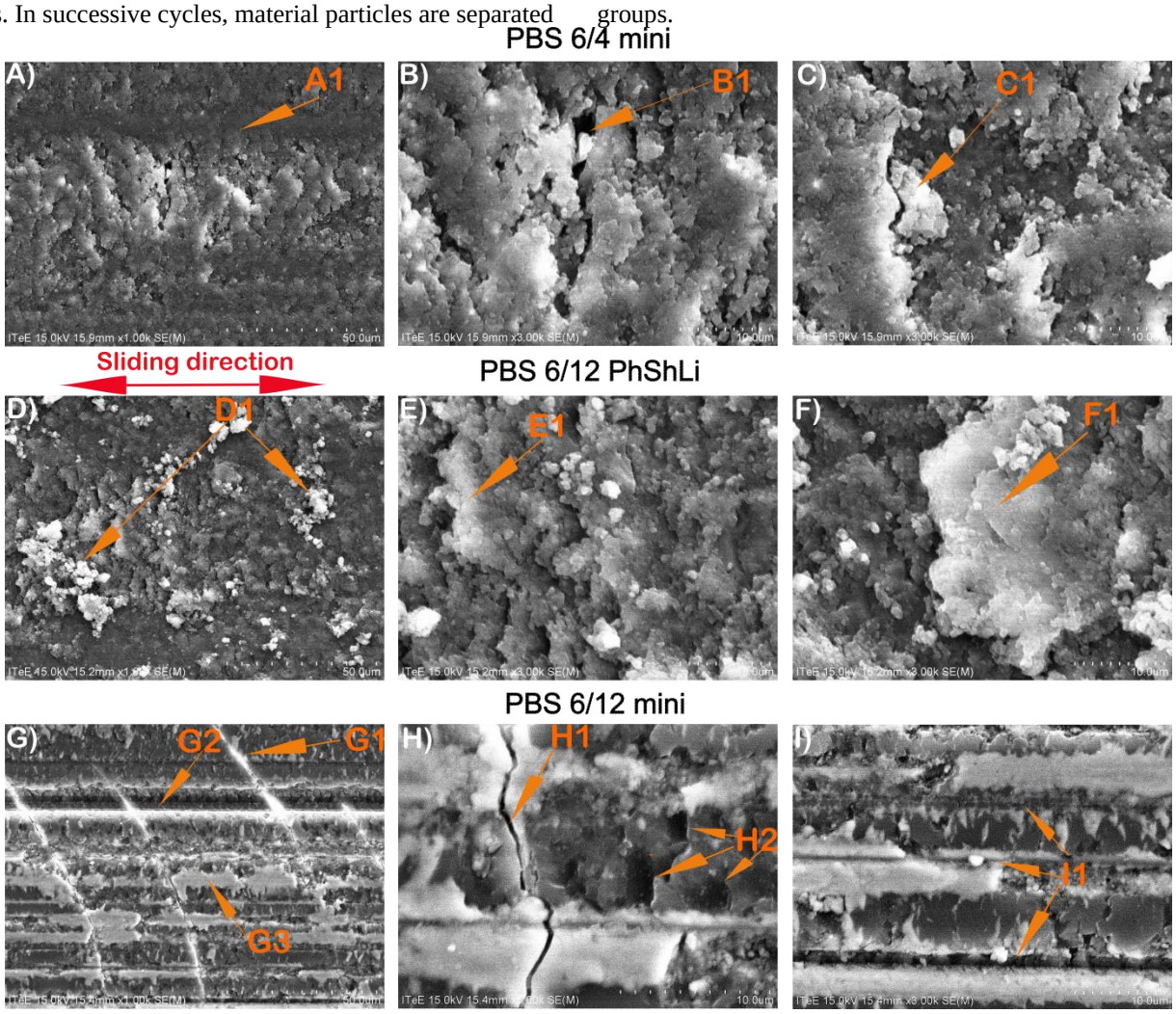

Fig. 17. SEM images of the friction track of the samples tested under sliding friction in reciprocating linear motion: A1 – furrow in line with the direction of friction force vector, B1 – material defects, C1 – separated material particle, D1 – loose particle agglomerates, E1 – material particles displaced in the direction of friction, D1 – material flake formed in the process of plastic deformation and fatigue crack coalescence, G1 – extended arc-shaped fatigue microcrack (possibly related to buckling of the polymer material in front of the metal counter sample), G2 – deep furrow, G3 – smeared material, H1 – fatigue crack propagation at the material particle boundary, H2 – material defects (removed material particles), I1 – series of parallel furrows

4. Analysis and discussion of test results

Polymeric materials are cost-effective compared to other materials, such as metals and ceramics, and are suitable for "low-cost applications" (Rashid, et al., 2021). Also, the cost-effectiveness of 3D printing techniques from polymeric materials is favourable, and the availability of printing materials and equipment is high. The continued development of AM methods from polymers launched a new era of manufacturing in several industrial sectors, including biomedicine, construction, electronics, telecommunications, mechanics and defence (Rashid, et al., 2021; Ahangar, et al., 2019). The wide range of applications results in the need to optimise AM process

conditions and starting material parameters (Ahangar, et al., 2019). Research and analysis in this area must be appropriate for the anticipated applications. For example, in the case of many devices where operational reliability is required, it can be provided by the addition of spare parts (Jabłońska, et al., 2023). Another application area is the manufacture of readily available and relatively inexpensive spare parts operating in structural nodes where sliding friction is present. The PBS material under study is popular and available in very many countries. Its price is not excessive, the cost of purchasing 0.5 kg is a few tens of euros. The description of the material states that it is characterised by high hardness, toughness and resolution (www.3dprintersbay, November 2023, which may determine potential application areas.

Due to the good tribological properties of polymer materials, such as self-lubrication, low friction coefficient over steel, and wear resistance, polymers are among the most widely used sliding materials (Kowalewski, 2019). However, the reliability of polymeric components made using the AM technology under the operating conditions of a kinematic node is difficult to predict and impossible to determine analytically. Therefore, experimentally determined properties that can be compared between manufacturers and testing laboratories are important. The hardness of a polymeric material is a measure of its resistance to contact concentrated forces. The impact of these forces can lead to permanent damage through local deformation of the material. Therefore, hardness is considered a performance property of the material. This characteristic value is an integral component of engineering theory and practice. Measurement of hardness is widely used, and various measurement methods have been developed. Many manufacturers of commercial polymeric materials for AM ensure the declared hardness. In the case of hard polymers, Shore durometer hardness measurement has become widespread in the industry. Therefore, at the beginning of research presented in the paper, reference was made to this surface parameter. In our study, hardness results characterising hard polymer materials were obtained. All samples achieved an average hardness of more than 80 Shore degree D (ShD), when the hardness declared by the manufacturer is 72 ShD (www.fepshop; November 2023b). The differences in the average hardness between groups of samples are small. Therefore, a non-parametric Wilcoxon test was carried out. This test was chosen due to the non-confirmation of a normal distribution in the Shore hardness result groups of. The Wilcoxon statistical test allows comparison of means in groups defined by the parameters of sample manufacture. Table 8 shows the value of the *T-statistic* and the *p-statistic* (the significance level $\alpha \leq 0.05$ was adopted).

Table 8. Wilcoxon test results for Shore hardness

Comparison of sample groups	T	p
PBS 6/4 PSM & PBS 6/12 PSM	85.00	0.4553
PBS 6/12 PSL & PBS 6/4 PSM	24.50	**0.0026**
PBS 6/12 PSL & PBS 6/12 PSM	33.00	**0.0072**

Statistically significant differences are marked in red. The results of the Wilcoxon test showed statistically significant differences between the Shore hardness of samples made with the PSL printer and those made with the PSM. However, post-processing parameters did not affect the differences in Shore hardness of samples made with the PSM printer.

Spare parts made using the DLP technology are precisely manufactured at a relatively high resolution. In this article, the PSL printer was characterised by a higher resolution. A study by a leading global manufacturer of polymer plain bearings (www.igus, November 2023a) reported that gears with a tooth modulus of 0.2 can be successfully manufactured using the DLP technology. In addition, the same manufacturer has released a product for manufacturing mechanism parts using the DLP technology (www.igus, November 2023b). Therefore, the manufacturing of parts operating in the kinematic nodes of small and micro machines and precision devices is justified and being developed. In such application areas, it seems that microindentation properties are crucial to the performance characteristics of parts made with the DLP technology. In microindentation tests conducted with a Vickers indenter, a greater variation in test results was obtained than in the Shore D macroindentation test. In addition, the ratio of quantities measured in the microindentation test can be of crucial use. Some researchers use the *H/E* ratio (Matthews, et al., 2006) (indentation hardness expressed in MPa) to indentation surface elastic modulus in MPa based on (Hardiman, et al., 2016; Sneddon, 1965). This ratio combines the ability to maximise elastic deformation (low modulus) and the ability to minimise permanent deformation (high hardness) (Pieniak, et al., 2020a). Researchers also use the H^2/E coefficient, defined by the ratio of the square of intrinsic hardness to the elastic modulus (Hardiman, et al., 2016; Oliver, et al., 2004; Pieniak, et al., 2020b). The H^2/E coefficient expresses the *elastic strain to failure.* The literature shows that the higher the value of H^2/E, the higher the wear resistance of the material (Nishimori, et al., 2021). The calculation results of *H/E* and H^2/E coefficients are shown in Figures 17a and 17b.

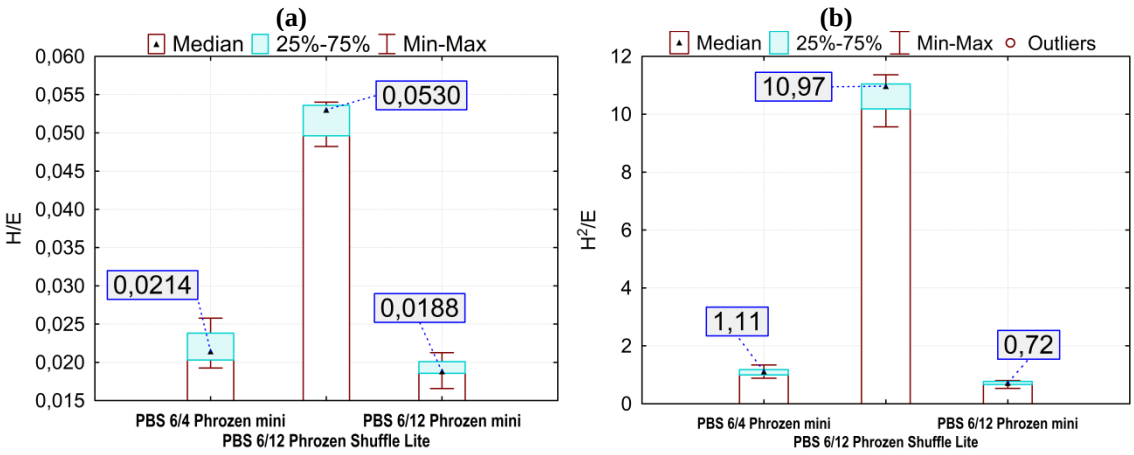

Fig. 18. Box-plot of H/E **(a)** and H^2/E **(b)** ratio calculation results

An analysis of the box-plots (Figure 18) shows that the calculation of both coefficients indicates the most favourable value for PBS 6/12 PSL samples. The higher value of coefficients may indirectly indicate greater durability at the sliding nodes. The significantly higher value of coefficients for the PBS 6/12 PSL samples may indicate a different relationship between the indentation hardness and the modulus of elasticity than that of the PSM samples. Figure 19 shows the relationship between the indentation hardness and the reduced modulus of elasticity of the surface. The equations of theoretical curves with the best fit to the distribution of empirical data are shown. The boxes show the value of correlation coefficient (r) and the fit to the linear model (p), which is low. A better fit was obtained using quadratic polynomials. In samples made with the PSM printer, the relationship between hardness and elastic modulus (Figures 19a and 19c) is close to directly proportional. However, in the case of samples made with the PSL printer (Figure 19b), it is close to inversely proportional, which translates into a negative correlation between hardness and elastic modulus. This means that for samples made with this printer, the elastic modulus decreases as hardness increases. The result obtained should be considered favourable in terms of surface qualities.

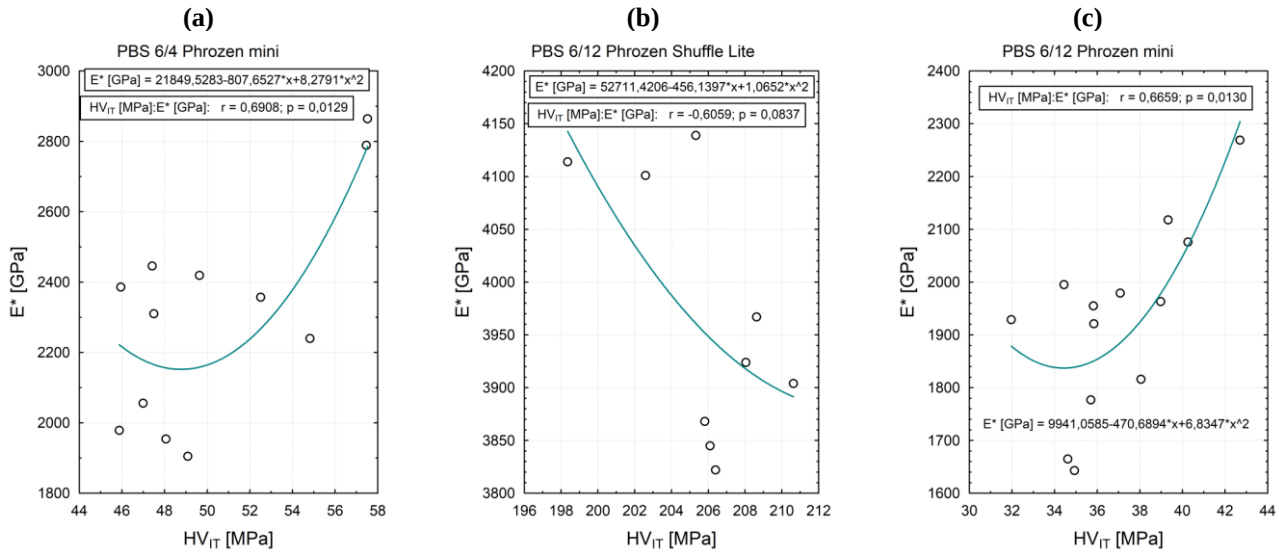

Fig. 19. Relationship between hardness (HV_{IT}) and reduced modulus of elasticity (E*):
(a) PBS_6/4_mini, **(b)** PBS_6/12_PSL, **(c)** PBS_6/12_PSM

Tribological applications for polymers include gears, a range of bearings, bearing cages and others. However, imperfections due to manufacturing make 3D polymers susceptible to fatigue damage (Catalin, 2019). The most popular 3D printing method – FDM – is characterised by a highly porous structure. The practical application of FDM parts is limited, due to the fact that they have more structural defects (Farahani, et al., 2016). DLP method is characterised by high resolution, fast performance, less shrinkage, and enables production of smooth surface elements (Wu, et al., 2015). The lower number of technological defects that characterise a DLP element should translate into higher fatigue life. In the case of samples of tested materials in rotary motion, intensive fatigue-like wear is accompanied by the stick-slip phenomenon, i.e. after

exceeding a certain limiting number of cycles, the friction coefficient increases by leaps and bounds (Figure 11) and stick-slip is observed. Only in the case of PBS 6/4 PSM under a normal load of 2 N, this phenomenon was not observed after the friction cycles < $20 \cdot 10^3$ (this number indicates the assumed durability of the PBS resin component). The results of tests on the microtribometer (Table 4) indicate that the difference between the maximum values of kinetic and static friction coefficient ("Start" in Table 4) allows the determination of the tendency to stick-slip (Popov, 2010). It turned out that under a normal load of 2 N, this ratio for the most durable of the PBS 6/4 PSM materials is close to number one. And in the case of PBS 6/12 PSM, it is about 3.75. In tests on the nanotribometer, reciprocating friction was performed. In a reciprocating friction test, the adhesive friction at each change of direction (momentary stop) alternates with the motion (sliding) friction between the two endpoints (Hanon, et al., 2022) in a friction cycle. The peak values presented in the graph (Figure 11) and in Table 5 were determined in successive friction cycles over the full range of the expected durability of the replacement part made of PBS ($20 \cdot 10^3$ cycles). The curves for PBS 6/4 PSM and PBS 6/12 PSL samples are similar in terms of course. In contrast, the curve for PBS 6/12 PSM is characterised by high friction coefficient values in the first cycles. In the paper (Hanon, et al., 2022), it is reported that friction coefficient values between 0.4 and 0.5 are considered not small (but in the range typical for plastics). The peak values of the friction coefficient achieved in the PBS 6/12 PSM test exceed this range and even reach 0.9. This means that the adaptation of contacting surfaces is hindered. A similar relation was shown in tribological tests of Nylon6 and ABS printed using FDM technology. An initial increase in the friction coefficient was observed, followed by a sharp decrease. This low friction regime is further followed up by a progressively delayed running-in period reaching a COF value of 0.42 (Boparai, et al., 2015). The transfer of the polymer material to the metal surface, which is typical of polymer-metal tribocontacts, occurs slowly and to a limited extent, as evidenced, among others, by the high abrasive wear of the ball. However, as reported in the paper (Myshkin, et al., 2005), it is apparent in the case of steel-polymer tribocontacts. There is no doubt that the wear seems too high, the degree of damage to the metal surface (Figure 14) is unacceptable under the conditions of contact with a cheaper polymer spare part. However, the formation of a polymer film on the metal ball is not quite excluded in the tested tribocontact. Smeared polymer particles can be seen on the counter sample in contact with PBS 6/12 PSL (Figure 14). The formation of polymer film is very important, and even if it does not last throughout the friction cycles, it has an important role. A transfer film is subsequently formed on the counter surface and if stable enough, it contributes to a reduction in the coefficient of friction (Dangnan, et al., 2020). It causes the formation of a polymer-polymer tribocontact for a certain period of time. After about $15 \cdot 10^3$ cycles, a clear change in the intensity of increase in the friction coefficient can be seen in all material groups. At the end of reciprocating friction test, it reaches values of about 0.7 and 0.8 for PBS 6/12 PSL samples.

The advantage of manufactured elements using DLP 3D printing technology is their low anisotropic behavior. Studies show no clear differences within the printing orientation (Grymak, et al., 2022). This material property is an advantage for elements manufactured using DLP printing technology, and may also translate into uniformity of contact strength and tribological properties. To improve the tribological properties, attempts were made to add graphene particles to the polymer resin used in DLP technology. A significant decrease in the friction coefficient of samples containing 0.5 wt% graphene was observed. It decreased by approximately 50% compared to the pure resin material (Hanon, et al., 2022). Mixing graphene particles with the resin requires additional laboratory equipment, including: precision weighing devices and vortex mixer. Basic knowledge in this field is also necessary. Researchers produced only a small amount of the composite at a time, which may be a technological limitation in some cases. In addition, such material will be more expensive. However, this may be one of the directions of development of sliding materials produced using DLP technology. There are also other technologies to improve sliding properties. An innovative solution was presented in (Wu, et al., 2023), they are more advanced, but on the other hand, they are more expensive.There is a postulated need to study the influence of various parameters affecting the friction and wear of AM-manufactured parts, such as load, speed, sliding distance, etc. (Rouf, et al., 2022). This work expands the state of knowledge in this area.

Poor mechanical properties of the developed parts and surface quality limit the use of 3D printed parts for various critical applications. However, these challenges can be overcome by examining the effects of various process parameters on mechanical properties and developing processes so that the production of products with appropriate properties can be more efficient (Rouf, et al., 2022). The authors believe that the implementation of 3D printing technology on a wider, even industrial scale, will continue. Difficulties result from incomplete knowledge about, among others, about operational properties. This direction should be pursued and the authors intend to focus on it in subsequent works.

5. Conclusions

Based on the research and analysis, the following final conclusions were drawn:

1. Conclusions regarding frictional and wear properties are very complex and, as shown, require experimental studies. It is difficult to objectively evaluate by workshop test methods (Shore hardness) the mechanical resistance and durability of surfaces under application conditions in a kinematic node.
2. The average Shore hardness value used in the comparative evaluation does not reflect the surface properties of the popular material used in the 3D DLP incremental technology. It seems that other quantities determined in this paper should be taken into account in the assessment of operational suitability.

3. Practical confrontation of the obtained results with those obtained by other researchers is hampered by the relatively small number of sources and the multiplicity, as well as the considerable diversity of materials and printing devices used in the AM technology.
4. Tests confirmed that the optimisation of the printing process in successive evolutions of printing devices is not always aimed at improving performance.
5. The results of friction tests are varied. Their analysis is complex. Taking into account the wear of both components of the friction pair – ball and disc –the PBS 6/4 PSM samples, for which the additional exposure after rinsing in alcohol was the shortest, were characterised by the highest durability. Although this was not obvious, the reduction in exposure time after alcohol cleaning proved beneficial in terms of performance properties of the tribocontact with a metal component.
6. Tribological tests in linear motion showed the lowest disc wear for PBS 6/12 PSM. However, in view of the assumed concept, as per which the cheap and temporarily used spare parts were to be printed of a polymer material, the wear of the metal ball was unacceptable.
7. The research hypothesis assumed that the functional properties do not differ depending on the type of printing device and exposure time in post-processing. In relation to the presented research and analyses, the hypothesis must be rejected.
8. What is new is the research problem regarding the use of a widely available and relatively cheap commercial material and the widely available and cheap DLP 3D printing technology for the production of metal-polymer friction node elements. The research was conducted in a way that enabled the identification of favorable parameters of DLP technology and post-processing, due to contact strength and durability. Similar research has not been conducted and the work expands the state of knowledge.

Reference

Ahangar, P., Cooke, M. E., Weber, M. H., & Rosenzweig, D. H., 2019. Current biomedical applications of 3D printing and additive manufacturing. Applied sciences, 9(8), 1713. DOI: 10.3390/app9081713

Abdelbary, A., 2014. Sliding mechanics of polymers. DOI: 10.1533/9781782421788.37

Abdelbary, A., 2015. Wear of polymers and composites. Woodhead Publishing. DOI: 10.1533/9781782421788.1

Ashby, M.F., 2011a. Materials selection—the basics, Materials Selection in Mechanical Design, 97-124.

Ashby, M., Shercliff, H., Cebon, D., 2011b. Inżynieria materiałowa. Galaktyka, Łodź.

Aziz, R., Haq, M. I. U., & Raina, A., 2020. Effect of surface texturing on friction behaviour of 3D printed polylactic acid (PLA). Polymer Testing, 85: 106434.

Boparai, K., Singh, R., & Singh, H., 2015. Comparison of tribological behaviour for Nylon6-Al-Al2O3 and ABS parts fabricated by fused deposition modelling: This paper reports a low cost composite material that is more wear-resistant than conventional ABS. Virtual and Physical Prototyping, 10(2), 59-66. DOI: 10.1080/17452759.2015.1037402

Capanidis, D., 2013. Mechanizm tarcia i zużywania wieloskładnikowych kompozytów na osnowie polioksymetylenu. Oficyna Wydawnicza Politechniki Wrocławskiej, Wrocław, 7-10.

Carneiro, O. S., Silva, A. F., & Gomes, R., 2015. Fused deposition modeling with polypropylene. Materials & Design, 83, 768-776. DOI: 10.1016/j.matdes.2015.06.053

Catalin, M., 2019. Overview of non-destructive evaluation techniques for metal-based additive manufacturing. Materials Science and Technology, 35:9: 1007-1015. DOI: 10.1080/02670836.2019.1596370

Dangnan, F., Espejo, C., Liskiewicz, T., Gester, M., & Neville, A., 2020. Friction and wear of additive manufactured polymers in dry contact. Journal of Manufacturing Processes, 59: 238-247. DOI: 10.1016/j.jmapro.2020.09.051

Dawoud, M., Taha, I., & Ebeid, S. J., 2015 Effect of processing parameters and graphite content on the tribological behaviour of 3D printed acrylonitrile butadiene styrene: Einfluss von Prozessparametern und Graphitgehalt auf das tribologische Verhalten von 3D-Druck Acrylnitril-Butadien-Styrol Bauteilen. Materialwissenschaft und Werkstofftechnik, 46(12), 1185-1195. DOI: 10.1002/mawe.201500450

Farahani, R.D., Dubé, M., & Therriault, D., 2016. Three-dimensional printing of multifunctional nanocomposites: manufacturing techniques and applications. Advanced materials, 28(28), 5794-5821. DOI: 10.1002/adma.201506215

Gil, L., Przystupa, K., Pieniak, D., Kozłowski, E., Antosz, K., Gauda, K., & Izdebski, P., 2021. Influence of contamination of gear oils in relation to time of operation on their lubricity. Applied Sciences, 11(24). DOI: 10.3390/app112411835

Grymak, J.N. Waddell, J.M. Aarts, S. Ma, J.J.E. 2022. Choi Evaluation of wear behaviour of various occlusal splint materials and manufacturing processes J. Mech. Behav. Biomed. Mater., 126. DOI: 10.1016/j.jmbbm.2021.105053

Hanon, M.M., Ghaly, A., Zsidai, L., & Klebert, S., 2022. Tribological characteristics of digital light processing (DLP) 3D printed graphene/resin composite: Influence of graphene presence and process settings. Materials & Design, 218. DOI: 10.1016/j.matdes.2022.110718

Hardiman, M., Vaughan, T. J., & McCarthy, C. T., 2016. The effects of pile-up, viscoelasticity and hydrostatic stress on polymer matrix nanoindentation. Polymer Testing, 52, 157-166. DOI: 10.1016/j.polymertesting.2016.04.003

https://3dpartnershop.com/product/phrozen-standard-resin-beige/?v=9b7d173b068d, November 2023.

https://fepshop.com/shop/printers/phrozen-shuffle-lite, November 2023.

https://fepshop.com/shop/materials/phrozen-standard-beige-0-5kg, November 2023.

https://phrozen3d.com/en-fr/pages/wash-cure-kit, November 2023.

https://www.3djake.pl/phrozen/sonic-mini, November 2023.

https://www.3dprintersbay.com/phrozen-beige-flex, November 2023.

https://www.igus.pl/info/3d-printing-resin-dlp, November 2023.

https://www.igus.pl/product/21071?artNr=I3000-PR-1000, November 2023.

Jabłońska, M., Jurczak, W., Ozimina, D., Adamiak, M., 2023. Increasing the operational reliability of a ship by using a composite impeller in the event of hydrophore pump failure. Eksploatacja i Niezawodnosc – Maintenance and Reliability, 25(1). DOI: 10.17531/ein.2023.1.18

Jandyal, A., Chaturvedi, I., Wazir, I., Raina, A., & Haq, M. I. U., 2022. 3D printing–A review of processes, materials and applications in industry 4.0. Sustainable Operations and Computers, 3, 33-42. DOI: 10.1016/j.susoc.2021.09.004

Kałdoński, T., 2020. Abrasive wearing processes of hydraulic precise pairs. Redakcja Wydawnictw WAT.

Kim, J.E., Choi, W.-H., Lee, D., Shin, Y., Park, S.-H., Roh, B.-D., Kim, D., 2021. Color and translucency stability of three-Dimensional printable dental materials for crown and bridge restorations. Materials, 14, 650. DOI: 10.3390/ma14030650

Kowalewski, P., 2019. Tarcie polimerów termoplastycznych w warunkach złożonego ruchu. OWPWr, Wrocław.

Krzyzak, A., Racinowski, D., Szczepaniak, R., Kosicka, E., 2023. An assessment of the reliability of CFRP composites used in nodes of friction after impact of UV-A impacts and thermal shocks, Eksploatacja i

Niezawodnosc – Maintenance and Reliability, 25(4). DOI: 10.17531/ein/174221

Lawrowski, Z., 2008. Tribologia. Red. Wrocław: Politechnika Wrocławska, 327.

LeBlanc, J., Shattuck, L., Warner, E., Javier, C., Chenwi, I., Chu, T., & Shukla, A., 2023. Effect of high pressure salt water absorption on the mechanical characteristics of additively manufactured polymers. International Journal of Lightweight Materials and Manufacture, 6(3), 379-391. DOI: 10.1016/j.ijlmm.2022.12.001

Lim, W.B., Bae, J. H., Seo, M. J., Min, J. G., Lee, J. H., Kim, S. H., ... & Huh, P., 2022. A novel UV-curable acryl-polyurethane for flexural 3D printing architectures. Additive Manufacturing, 51, 102625. DOI: org/10.1016/j.addma.2022.102625

Matthews, A., Leyland, A., 2006. The role of nanocomposite coatings in surface engineering. In 5th International Surface Engineering Conference, 1-5, ASM International.

Mitchell, A., Lafont, U., Hołyńska, M., & Semprimoschnig, C. J. A. M., 2018. Additive manufacturing—A review of 4D printing and future applications. Additive Manufacturing, *24*, 606-626. DOI: 10.1016/j.addma.2018.10.038

Mohammed, J.S., 2016. Applications of 3D printing technologies in oceanography, Methods Oceanogr., 17, 97–117.

Mohamed, O.A., Mohamed, O. A., Masood, S. H., Bhowmik, J. L., & Somers, A. E., 2017. Investigation on the tribological behavior and wear mechanism of parts processed by fused deposition additive manufacturing process. Journal of Manufacturing Processes, 29, 149-159. DOI: 10.1016/j.jmapro.2017.07.019

Müller, M., Valášek, P., Kolář, V., Šleger, V., Gürdil, G. A. K., Hromasová, M., ... & Pexa, M., 2019. Material utilization of cotton post-harvest line residues in polymeric composites. Polymers, 11(7). DOI: 10.3390/polym11071106

Myshkin, N.K., Petrokovets, M. I., Kovalev, A. V., 2005. Tribology of polymers: Adhesion, friction, wear, and mass-transfer. Tribology International, 38(11-12), 910-921. DOI: 10.1016/j.triboint.2005.07.016

Nishimori, F., Ikeshima, D., Kanamori, K., Yamamura, H., & Yonezu, A., 2021. Characterization of the surface degraded layer of polymers using an indentation method. Materials Today Communications, 26, 101873. DOI: 10.1016/j.mtcomm.2020.101873

Oliver, W.C., & Pharr, G.M., 2004. Measurement of hardness and elastic modulus by instrumented indentation: Advances in understanding and refinements to methodology. Journal of materials research, 19(1), 3-20.

Ozimina D., Ryniewicz A., 2013. Eksploatacja systemów tribologicznych. T. 1, Znaczenie tribologii w eksploatacji obiektów technicznych, Kielce.

Pieniak, D., Gauda, K., 2020a. Indentation Hardness and Tribological Wear in Conditions of Sliding Friction of the Surface Layer of Composites Based on Methacrylate Resins with Ceramic Nanofiller. Advances in Science and Technology Research Journal, 14(2), 112-119. DOI: 10.12913/22998624/118867

Pieniak, D., Niewczas, A., Walczak, A., Łępicka, M., Grądzka-Dahlke, M., Maciejewski, R., Kordos, P., 2020b, The effect of thermal stresses on the functional properties of various dental composites. Tribol. Int., 152, 106509, DOI: 10.1016/j.triboint.2020.106509.

PN-EN ISO 14577-1:2015-09 Metale - Instrumentalna próba wciskania wgłębnika do określania twardości i innych własności materiałów.

PN-EN ISO 868:2005 Tworzywa sztuczne i ebonit - Oznaczanie twardości metodą wciskania z zastosowaniem twardościomierza (twardość metodą Shore'a).

Pokorska, I., Tacikowski, M., Moskalow, M., & Wierzchoń, T., 2014. Mikrostruktura i właściwości dyfuzyjnych warstw na bazie chromu na stopie magnezu AZ91D. Inżynieria Materiałowa, 35, 6, 540-543.

Popov, V.L., 2010. Contact mechanics and friction. Berlin: Springer Berlin Heidelberg, 231-253. DOI: 10.1007/978-3-642-10803-7

Qu, A., & Li, F., 2023. Influence of 3D printing on compressor impeller fatigue crack propagation life. International Journal of Mechanical Sciences, 245. DOI: 10.1016/j.ijmecsci.2023.108107

Ramadan, M. A., 2022. Tribological investigations of 3D Printed Polymers and Their Applications. A Review. Journal of Modern Industry and Manufacturing, 1(1), 1-9. DOI: 10.53964/jmim.2022002

Rashid, A. A., & Koç, M., 2021. Fused filament fabrication process: a review of numerical simulation techniques. Polymers, 13(20). DOI: 10.3390/polym13203534

Rezaie, F., Farshbaf, M., Dahri, M., Masjedi, M., Maleki, R., Amini, F., Wirth, J., Moharamzadeh, K., Weber, F. E., Tayebi, L., 2023. 3D Printing of Dental Prostheses: Current and Emerging Applications. J. Compos. Sci., 7, 80. DOI: 10.3390/jcs7020080

Romek, D., Selech, J., Ulbrich, D. P., Felusiak, A., Kieruj, P., Janeba-Bartoszewicz, E., 2020. The impact of padding weld shape of agricultural machinery tools on their abrasive wear. Tribologia, 2, 55-62.

Rouf, S., Raina, A., Haq, M. I. U., Naveed, N., Jeganmohan, S., & Kichloo, A. F., 2022. 3D printed parts and mechanical properties: Influencing parameters, sustainability aspects, global market scenario, challenges and applications. Advanced Industrial and Engineering Polymer Research, 5(3), 143-158. DOI: 10.1016/j.aiepr.2022.02.001

Shafi, W.K., Raina, A., Ul Haq, M. I., 2018. Friction and wear characteristics of vegetable oils using nanoparticles for sustainable lubrication. Tribology-Materials, Surfaces & Interfaces, 12(1), 27-43. DOI: 10.1080/17515831.2018.1435343

Skoć, A., Spałek, J., Markusik, S., 2008. Podstawy konstrukcji maszyn Vol. 2. ed. Warszawa: Wydawnictwo WNT, 603.

Smal, T., 2006. Naprawa uszkodzeń bojowych sprzętu wojskowego z zastosowaniem kompozytów klejowych. Eksploatacja Uzbrojenia i Sprzętu Wojskowego. Problemy Obsługiwania Techniki Lądowej w Siłach Zbrojnych RP. Wrocław, 205-210.

Sneddon, I.N., 1965. The relation between load and penetration in the axisymmetric Boussinesq problem for a punch of arbitrary profile. International journal of engineering science, 3(1), 47-57.

Snyder, T., Mick, J., Weislogel, M., Beyl, M., Buchholz, A., Molina, E., & Vu, J., 2015. Single-build additive manufacturing of autonomous machines. NIP & Digital Fabrication Conference. Society for Imaging Science and Technology, 31, 293-298.

Topolinski, T., 1997. Analiza teoretyczna i badania kumulacji uszkodzen zmeczeniowych konstrukcyjnych kompozytow polimerowych. Rozprawy. Akademia Techniczno-Rolnicza w Bydgoszczy, 82, 1-112.

Wang, Q., Wang, Y., Wang, H., Fan, N., Yan, F., 2016. Experimental investigation on tribological behavior of several polymer materials under reciprocating sliding and fretting wear conditions. Tribology International, 73-82. DOI: 10.1016/j.triboint.2016.08.030

Wang, Y., Li, X., Chen, Y., Zhang, C., 2021. Strain rate dependent mechanical properties of 3D printed polymer materials using the DLP technique. Additive Manufacturing, 47. DOI: 10.1016/j.addma.2021.102368

Wu, G.H., Hsu, S.H., 2015. Polymeric-based 3D printing for tissue engineering. Journal of medical and biological engineering, 35, 285-292. DOI: 10.1007/s40846-015-0038-3

Wu, P., Yu, T., Li, G., Chen, M., 2023. Magnetic field-assisted DLP of CIPs/resin composites: Mechanical properties, anisotropic magnetic performance and wear behavior. Wear, 523. DOI: 10.1016/j.wear.2023.204800

Zhang, B., Huang, W., Wang, J., Wang, X., 2013e al. Comparison of the effects of surface texture on the surfaces of steel and UHMWPE. Tribology International, 65, 138-145. DOI: 10.1016/j.triboint.2013.01.004